

RELIABLE IDENTIFICATION OF COMPTON-THICK QUASARS AT $z \approx 2$: *SPITZER* MID-INFRARED SPECTROSCOPY OF HDF-oMD49

D. M. ALEXANDER,¹ R.-R. CHARY,² A. POPE,^{3,4,5} F. E. BAUER,⁶ W. N. BRANDT,⁷ E. DADDI,⁸
M. DICKINSON,⁵ D. ELBAZ,⁸ AND N. A. REDDY⁵

Received 2008 March 10; accepted 2008 July 10

ABSTRACT

Many models that seek to explain the origin of the unresolved X-ray background predict that Compton-thick active galactic nuclei (AGNs) are ubiquitous at high redshift. However, few distant Compton-thick AGNs have been reliably identified to date. Here we present *Spitzer* IRS spectroscopy and 3.6–70 μm photometry of a $z = 2.211$ optically identified AGN (HDF-oMD49) that is formally undetected in the 2 Ms *Chandra* Deep Field–North (CDF-N) survey. The *Spitzer* IRS spectrum and spectral energy distribution of this object is AGN dominated, and a comparison of the energetics at X-ray wavelengths to those derived from mid-infrared (mid-IR) and optical spectroscopy shows that the AGN is intrinsically luminous ($L_{2-10\text{ keV}} \approx 3 \times 10^{44}$ ergs s^{-1}) but heavily absorbed by Compton-thick material ($N_{\text{H}} \gg 10^{24}$ cm^{-2}); i.e., this object is a Compton-thick quasar. Adopting the same approach that we applied to HDF-oMD49, we found a further six objects at $z \approx 2-2.5$ in the literature that are also X-ray weak/undetected but have evidence for AGN activity from optical and/or mid-IR spectroscopy, and show that all of these sources are likely to be Compton-thick quasars with $L_{2-10\text{ keV}} > 10^{44}$ ergs s^{-1} . On the basis of the definition of Daddi et al., these Compton-thick quasars would be classified as mid-IR excess galaxies, and our study provides the first spectroscopic confirmation of Compton-thick AGN activity in a subsample of these $z \approx 2$ mid-IR-bright galaxies. Using the four objects that lie in the CDF-N field, we estimate the space density of reliably identified Compton-thick quasars [$\Phi \approx (0.7-2.5) \times 10^{-5}$ Mpc^{-3} for $L_{2-10\text{ keV}} > 10^{44}$ ergs s^{-1} objects at $z \approx 2-2.5$] and show that Compton-thick accretion was probably as ubiquitous as unobscured accretion in the distant universe.

Subject headings: galaxies: active — galaxies: high-redshift — infrared: galaxies — ultraviolet: galaxies — X-rays: galaxies

Online material: color figures

1. INTRODUCTION

There is a growing need for a complete census of active galactic nuclei (AGNs). The seminal discovery that every massive galaxy in the local universe harbors a supermassive black hole ($M_{\text{BH}} \gtrsim 10^6 M_{\odot}$) implies that all massive galaxies must have hosted AGN activity at some time during the past ≈ 13 Gyr (e.g., Rees 1984; Kormendy & Richstone 1995). To trace accurately how and when these black holes grew requires a detailed census of AGN activity that will provide, among other things, estimates of the efficiency and duty cycle of black hole growth and any dependencies of nuclear obscuration on AGN luminosity, redshift, and host galaxy type (e.g., Marconi et al. 2004; La Franca et al. 2005; Shankar et al. 2008).

The exceptional sensitivity of the *Chandra* Deep Field observations (e.g., Brandt et al. 2001; Giacconi et al. 2002; Alexander et al. 2003b) has helped to unveil a >10 times larger population of AGNs than found at most other wavelengths (≈ 7200 deg^{-2} ;

e.g., Bauer et al. 2004). Optical spectroscopic follow-up observations have shown that these AGNs are detected out to $z \approx 5$, and detailed X-ray spectral analyses have revealed that the majority of the sources are obscured by gas and dust (e.g., Barger et al. 2003; Szokoly et al. 2004; Tozzi et al. 2006; see Brandt & Hasinger [2005] for a review). However, although clearly effective at identifying even heavily obscured AGNs out to high redshift, there is compelling evidence that a large fraction of the AGN population remains undetected at the <10 keV observed-frame energies probed by these surveys: (1) about half of the X-ray background (XRB) is unresolved at >6 keV (Worsley et al. 2005); (2) the *observed* obscured : unobscured AGN ratio is lower than that found for comparably luminous AGNs in the local universe (e.g., Treister & Urry 2005); (3) the 5–10 keV blank-field number counts are steeply rising at the faintest X-ray fluxes (Rosati et al. 2002); and (4) few Compton-thick AGNs ($N_{\text{H}} \gtrsim 1.5 \times 10^{24}$ cm^{-2}) have been identified, even though they comprise $\approx 50\%$ of the AGN population in the local universe (e.g., Risaliti et al. 1999; Guainazzi et al. 2005; Tozzi et al. 2006).

Many of the X-ray-undetected AGNs are expected to be intrinsically luminous sources that are heavily obscured by Compton-thick material (i.e., $N_{\text{H}} > 1.5 \times 10^{24}$ cm^{-2} ; see Comastri [2004] for a review). The most robust identification of a Compton-thick AGN is made from high signal-to-noise ratio (S/N) X-ray spectroscopy, where the detection of a high equivalent width Fe K emission line ($W_{\lambda} > 1$ keV at rest-frame energies 6.4–6.9 keV) and a steeply rising reflection component at >10 keV reveals that little or no X-ray emission is being seen directly, implying that the central source is very heavily absorbed (e.g., George & Fabian 1991; Matt et al. 1996, 2000; Maiolino et al. 1998). However, since the extreme obscuration toward the nucleus of a Compton-thick

¹ Department of Physics, Durham University, Durham DH1 3LE, UK.

² *Spitzer* Science Center, California Institute of Technology, MS 220-6, Pasadena, CA 91125.

³ *Spitzer* Fellow.

⁴ Department of Physics and Astronomy, University of British Columbia, Vancouver, BC V6T 1Z1, Canada.

⁵ National Optical Astronomy Observatory, 950 North Cherry Avenue, Tucson, AZ 85719.

⁶ *Chandra* Fellow; Columbia Astrophysics Laboratory, Columbia University, Pupin Laboratories, 550 West 120th Street, New York, NY 10027.

⁷ Department of Astronomy and Astrophysics, Pennsylvania State University, 525 Davey Lab, University Park, PA 16802.

⁸ Laboratoire AIM, CEA/DSM-CNRS-Université Paris Diderot, Irfu, Orme des Merisiers, 91191 Gif-sur-Yvette, France.

AGN renders the observed <10 keV emission ≈ 30 – 1000 times fainter than the intrinsic (i.e., unabsorbed) emission, it is often challenging to identify robustly these sources on the basis of their X-ray data alone; the range of absorption correction factors is based on the observed-to-intrinsic X-ray luminosity ratio for the AGNs in Table 8.1 of Comastri (2004), with the observed X-ray fluxes from Bassani et al. (1999). For example, despite Compton-thick AGNs comprising half of the AGN population in the local universe, only ≈ 50 sources have been reliably identified from X-ray data to date (e.g., Comastri 2004). Fortunately, although not as conclusive as high S/N X-ray spectroscopy, the presence of Compton-thick absorption can also be identified in X-ray-weak AGNs when a reliable measurement of the intrinsic power of the AGNs is available at other wavelengths; we stress here the necessity for X-ray constraints in order to identify a Compton-thick AGN, since it is only in the X-ray band that an absorbing column density can be measured or inferred.

Two of the most reliable measurements of the intrinsic power of an obscured AGN are the luminosity of the mid-infrared (mid-IR; rest frame >3 μm ; e.g., Efstathiou & Rowan-Robinson 1995; Granato et al. 1997; Lutz et al. 2004) continuum and high-excitation emission lines (i.e., [O III] $\lambda 5007$; e.g., Allen 1973; Kwan & Krolik 1981; Bassani et al. 1999), both of which are believed to be directly illuminated by the central source. These emission regions provide a good proxy for the intrinsic AGN luminosity, even in the presence of extreme Compton-thick absorption, since they are more extended than the X-ray-absorbing material (i.e., larger than the broad-line region; e.g., Lamer et al. 2003; Risaliti et al. 2007). As the luminosities of both the mid-IR continuum and the high-excitation emission-line region are dependent on many factors, including the location and geometry of the region with respect to the central source, more robust constraints are placed if both measurements are available.

Comprehensive evidence for a large X-ray-undetected AGN population has been found from a variety of X-ray-based analyses using sources detected in deep *Spitzer* surveys at mid-IR wavelengths, suggesting that Compton-thick AGNs may be ubiquitous in the distant universe (e.g., Donley et al. 2005, 2007; Alonso-Herrero et al. 2006; Polletta et al. 2006; Daddi et al. 2007b; Steffen et al. 2007; Martínez-Sansigre et al. 2007; Fiore et al. 2008). However, all of these studies have relied on photometric observations for the identification of candidate Compton-thick AGNs, leading to significant uncertainties in measurements of the intrinsic AGN luminosity, the absorbing column density, the degree of contamination from star formation activity, and by implication, the space density of distant Compton-thick AGNs. In this paper we present *Spitzer* Infrared Spectrograph (IRS) spectroscopy and 3.6 – 70 μm observations of an optically identified narrow emission-line AGN at $z = 2.211$ (HDF-oMD49; Steidel et al. 2002) that is undetected in the published catalogs of the deepest X-ray observation currently available (the 2 Ms *Chandra* Deep Field–North [CDF-N]; Alexander et al. 2003b). From a comparison of the AGN energetics at X-ray wavelengths to those determined from optical and mid-IR spectroscopy, we robustly show that HDF-oMD49 hosts an intrinsically luminous ($L_{2-10\text{keV}} \approx 3 \times 10^{44}$ ergs s^{-1}), Compton-thick AGN; i.e., this source is a Compton-thick quasar.⁹ We then use these X-ray–optical–mid-IR diagnostics to identify a further six

distant Compton-thick quasars in the literature and place limits on the space density of Compton-thick quasars at $z \approx 2$. We adopted $H_0 = 71$ km s^{-1} Mpc $^{-1}$, $\Omega_M = 0.27$, and $\Omega_\Lambda = 0.73$ throughout.

2. OBSERVATIONS

HDF-oMD49 (optical position $\alpha_{J2000.0} = 12^{\text{h}}37^{\text{m}}04.34^{\text{s}}$, $\delta_{J2000.0} = +62^\circ 14' 46.2''$; Steidel et al. 2002) was originally identified in the Lyman break galaxy (LBG) searches of Steidel et al. (2002, 2003). With a redshift of $z = 2.211$, HDF-oMD49 lies at the low-redshift end of the LBG population (median redshift $z \approx 3$). HDF-oMD49 is also identified as a BX/BM galaxy, based on the criteria of Steidel et al. (2004), and it is dubbed BM 1156 in the BX/BM study of Reddy et al. (2006). The apparent contradiction in HDF-oMD49 being selected as both an LBG and BX/BM is due to small differences in the photometric data used in these studies.

2.1. *Spitzer* Data

HDF-oMD49 is detected by the Infrared Array Camera (IRAC) at 3.6 – 8.0 μm and the Multiband Imaging Photometer for *Spitzer* (MIPS) at 24 μm in the *Spitzer* observations obtained as part of the Great Observatories Origins Deep Survey (GOODS) legacy project (PI: M. Dickinson; R. Chary et al. 2008, in preparation); the 3.6 , 4.5 , 5.8 , 8.0 , and 24 μm fluxes are 6.1 , 7.0 , 14.8 , 40.1 , and 380 μJy , respectively. Although HDF-oMD49 is bright at 24 μm , it is undetected in the ultra-deep 70 μm observations of Frayer et al. (2006; 3σ upper limit of $f_{70\mu\text{m}} < 2.0$ mJy), indicating that it has a “warm” mid-IR spectral energy distribution (SED; e.g., Papovich et al. 2007). HDF-oMD49 is also detected at 16 μm with $f_{16\mu\text{m}} = 222$ μJy using the “peak-up” imaging capability of *Spitzer* IRS (H. Teplitz et al. 2008, in preparation).

The *Spitzer* IRS spectroscopy of HDF-oMD49 was obtained in spectral staring mode as part of program GO2-20456 (PI: R. Chary) using the Long-Low (LL) modules ($R \approx 64$ – 128 ; Houck et al. 2004). HDF-oMD49 was observed with LL1 (20.5 – 37.9 μm) for 3 hr, and additional observations with LL1 (0.93 hr) and LL2 (1.33 hr; 14.3 – 21.2 μm) were obtained when HDF-oMD49 fell serendipitously into the slit of another target from the same program. We analyzed the two-dimensional basic calibrated data files from the S14.0.0 *Spitzer* IRS pipeline data; data reduction includes cleaning rogue pixels, fitting and removing the latent charge buildup, subtracting the sky, and averaging the two-dimensional files together. Spectral extraction was performed using a 2 pixel wide window in SPICE, and the data were calibrated using the same extraction window on a standard-star spectrum.¹⁰ The average rms of the LL1 and LL2 spectra are 97 and 120 μJy , respectively. The *Spitzer* IRS fluxes measured through the 16 and 24 μm filter spectral response curves are 180 ± 120 and 370 ± 100 μJy , respectively, consistent with the observed fluxes in these bands.¹¹ For more details on the observations and data reduction, see Pope et al. (2008).

2.2. *Chandra* Data

HDF-oMD49 is undetected in the published 2 Ms *Chandra* catalogs of Alexander et al. (2003b). However, these catalogs were produced using a conservative source detection algorithm to minimize the number of spurious detections, and it is possible to identify robustly fainter sources when searching for X-ray emission

⁹ Here we define a quasar as an AGN with $L_{2-10\text{keV}} \geq 10^{44}$ ergs s^{-1} . This definition is consistent with that derived from the classical optical quasar threshold of $M_B < -23$ (e.g., Schmidt & Green 1983), assuming the α_{OX} relationship of Steffen et al. (2006) and the composite quasar spectrum of Vanden Berk et al. (2001); this definition is also consistent with $L_{X,*}$ derived for X-ray-unobscured AGNs (see Table 5 of Hasinger et al. [2005]).

¹⁰ See <http://ssc.spitzer.caltech.edu/postbcd/spice.html> for details of SPICE.

¹¹ The spectral response curves for the individual *Spitzer* instruments can be obtained from <http://ssc.spitzer.caltech.edu/obs/>.

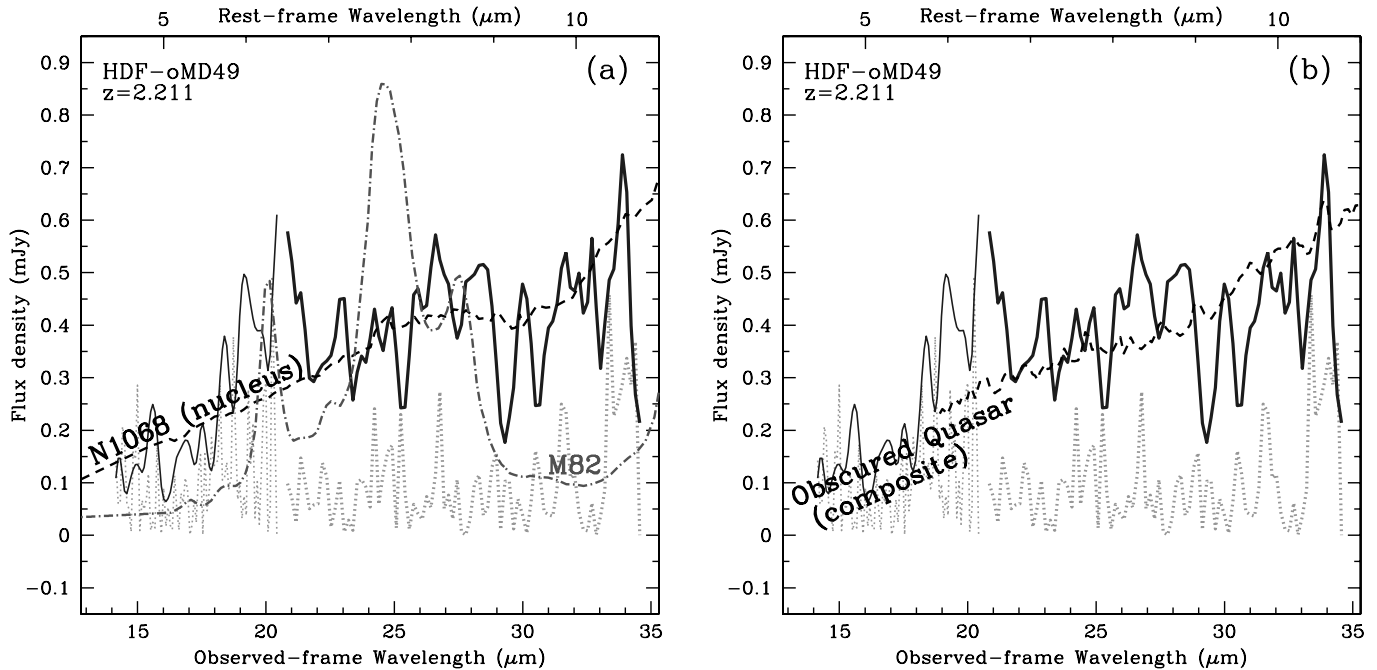


FIG. 1.— *Spitzer* IRS spectrum of HDF-oMD49 (solid line) for the LL1 (thick line) and LL2 (thin line) orders; the 1 σ error arrays are plotted as a dotted line. Comparison spectra: (a) the starburst galaxy M82 and the Compton-thick AGN NGC 1068; and (b) the composite spectrum of X-ray-obscured Compton-thin quasars from Sturm et al. (2006), are shifted to $z = 2.211$ and overlaid on the data of HDF-oMD49. The mid-IR spectrum of HDF-oMD49 is consistent with that of an AGN; see § 3.1 for quantitative constraints. [See the electronic edition of the *Journal* for a color version of this figure.]

associated with a known source (e.g., see § 3.4.2 of Alexander et al. [2003b] and § 5 of Alexander et al. [2001]). Indeed, adopting a WAVDETECT (Freeman et al. 2002) false-positive probability threshold of 10^{-5} we detected significant X-ray emission (X-ray position $\alpha_{J2000.0} = 12^{\text{h}}37^{\text{m}}04.32^{\text{s}}$, $\delta_{J2000.0} = +62^{\circ}14'46.4''$) within $0.25''$ of the optical position of HDF-oMD49 in the 0.5–8, 0.5–2, and 4–8 keV bands with 8.1 ± 3.5 , 6.7 ± 2.8 , and 4.9 ± 2.6 counts, respectively (see also Laird et al. 2006). HDF-oMD49 remains undetected in all of the other four X-ray bands explored by Alexander et al. (2003b), and we calculated 3 σ upper limits following § 3.4.1 of Alexander et al. (2003b). Although the S/N of the X-ray data is low, the low background of *Chandra* allows weak sources with very low count rates to be reliably detected. For example, with a measured background in the detection aperture of HDF-oMD49 (≈ 2 pixel radius) of only ≈ 1 counts in the 0.5–2 keV band, the probability of detecting ≈ 7 counts by chance is $\approx 10^{-5}$; furthermore, HDF-oMD49 is detected in two independent bands, increasing the overall probability that the detection is real.

The X-ray counts correspond to fluxes of 7.1×10^{-17} ergs $\text{s}^{-1} \text{cm}^{-2}$ (0.5–8 keV), 2.6×10^{-17} ergs $\text{s}^{-1} \text{cm}^{-2}$ (0.5–2 keV), and 1.5×10^{-16} ergs $\text{s}^{-1} \text{cm}^{-2}$ (4–8 keV), for $\Gamma = 1.4$ (i.e., the spectral slope of the XRB). The detection in the 4–8 keV band (rest frame 12.8–25.7 keV) is particularly notable, since *Chandra* is significantly less sensitive at 4–8 keV than at < 4 keV energies, suggesting that HDF-oMD49 has a flat X-ray spectral slope; the nondetection in the wider 2–8 keV band provides support for this hypothesis. The X-ray band ratio (the 2–8 keV/0.5–2 keV count rate ratio) is < 1.9 , which corresponds to $\Gamma > 0.2$ and is consistent with the X-ray spectral slope derived from the 4–8 keV/0.5–2 keV count rate ratio ($\Gamma \approx 0.4$); the difference in the X-ray fluxes estimated using $\Gamma = 0.4$ instead of $\Gamma = 1.4$ is negligible given the low S/N of the X-ray data ($\leq 15\%$). The corresponding rest-frame 1.6–6.4, 6.4–12.8, and 12.8–25.7 keV luminosities (or 3 σ upper limit) of HDF-oMD49 are 10^{42} , $< 4 \times 10^{42}$, and 6×10^{42} ergs s^{-1} , respectively.

3. RESULTS

3.1. The *Spitzer* SED

In Figure 1a we show the *Spitzer* IRS spectrum of HDF-oMD49. The spectrum is noisy, particularly in the LL2 order. However, there is no significant emission from the dominant rest-frame $7.7 \mu\text{m}$ polycyclic aromatic hydrocarbon (PAH) feature found in star-forming galaxies, indicating that the mid-IR spectrum does not have a strong contribution from star formation activity. By contrast, the *Spitzer* IRS spectrum of HDF-oMD49 is similar to the nearby Compton-thick AGN NGC 1068 and even shows weak evidence for Si absorption at $9.7 \mu\text{m}$, a feature often seen in obscured AGNs (e.g., Shi et al. 2006; Hao et al. 2007; Spoon et al. 2007). The *Spitzer* IRS spectrum of HDF-oMD49 is also qualitatively similar to the composite mid-IR spectrum of the X-ray-obscured quasars ($L_X > 10^{44}$ ergs s^{-1} ; $N_H > 10^{22}$ cm^{-2}) investigated by Sturm et al. (2006); see Figure 1b.

We can quantify the contributions from AGN and star formation activity to the mid-IR luminosity of HDF-oMD49 by fitting the *Spitzer* IRS spectrum with AGN and star formation templates. Adopting the approach of Pope et al. (2008), we fit the *Spitzer* IRS spectrum with an M82 starburst component and include an AGN component using the nuclear spectrum of NGC 1068, performing a χ^2 minimization to obtain the best-fitting normalization. On the basis of this approach, we find that the mid-IR spectrum of HDF-oMD49 is dominated by AGN activity, with a limit of a 10% contribution from star formation in the *Spitzer* IRS band; there is no clear signature for star formation, and this limit effectively corresponds to the noise per pixel in the spectra. We get consistent results if we fit the mid-IR spectrum with an M82 starburst component and an absorbed power-law component (to represent the AGN), leaving the slope of the power law and the extinction as free parameters. The best-fitting results with this second approach give a spectral slope of $\alpha = 2$ (consistent with that found for AGN-dominated sources; e.g., Alonso-Herrero et al. [2003], where

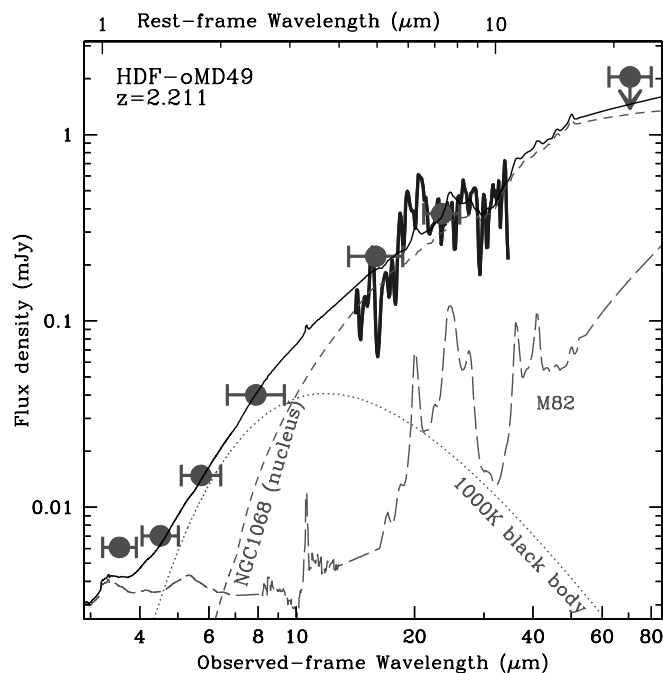


FIG. 2.—Infrared data of HDF-oMD49, showing the *Spitzer* IRS spectroscopy (thick solid curve) and *Spitzer* photometry (circles) at 3.6–70 μm . The error bar in the x -axis direction indicates the width that corresponds to >50% of the maximum transmission in each of the photometric bands; see footnote 3. The data are compared to the SEDs of the Compton-thick AGN NGC 1068 (dashed curve) and the starburst galaxy M82 (long-dashed curve), which are shifted to $z = 2.211$ and normalized based on the results from fitting the mid-IR spectrum of HDF-oMD49 (see § 3.1). In order to fit the data in the IRAC bands, it was necessary to also add a blackbody component of very hot 1000 K dust (dotted curve). The thin solid curve shows the combined model results. The data for the NGC 1068 and M82 SEDs were taken from Rigopoulou et al. (1999), Chary & Elbaz (2001), Galliano et al. (2003), and Magnelli et al. (2008). [See the electronic edition of the *Journal* for a color version of this figure.]

$f_{\nu} \approx \nu^{-\alpha}$) with $\tau_{9.7 \mu\text{m}} \approx 0.65$ and a $\approx 5\%$ limit on the contribution from star formation.

In Figure 2 we show the 3.6–70 μm SED of HDF-oMD49 and plot on the NGC 1068 and M82 templates, normalized to the values obtained from the mid-IR spectral fitting. The strong observed-frame 3.6–8 μm emission and the power-law-like, featureless SED strengthen our conclusion from the mid-IR spectral fitting, showing that the IR SED of HDF-oMD49 is dominated by AGN activity. The strongly rising continuum at $>4.5 \mu\text{m}$ (rest frame $>1.4 \mu\text{m}$) also indicates that the contribution from starlight (which typically peaks at rest frame 1.6 μm) is weak at these wavelengths. The combination of the NGC 1068 and M82 templates gives a respectable fit to the overall SED of HDF-oMD49, even though the wavelength coverage of the SED data is 3 times broader than that used when fitting the mid-IR spectrum (rest frame 1.1–21.8 μm vs. rest frame 4.4–10.6 μm). However, the combination of the NGC 1068 and M82 components lies below the observed emission in the IRAC bands (rest frame $<3 \mu\text{m}$). This excess emission can be fitted by adding a blackbody component of very hot dust ($\approx 1000 \text{ K}$), as often found in obscured AGNs (e.g., Alonso-Herrero et al. 2001). On the basis of the fitted NGC 1068 component, the rest-frame 6 μm luminosity from HDF-oMD49 is $\nu L_{6 \mu\text{m}} \approx 1.3 \times 10^{45} \text{ ergs s}^{-1}$ ($f_{6 \mu\text{m}} = 210 \mu\text{Jy}$), indicating that the AGN is powerful (e.g., compare to the nearby AGNs explored by Lutz et al. [2004]).

Our analyses show that the IR SED of HDF-oMD49 is dominated by AGN activity and allows for just a small contribution from star formation. Using the best-fitting star formation component

normalizations and the relationship between PAH luminosity and star formation rate (SFR) given by Pope et al. (2008; see their eq. [7]), we predict SFR of $\approx 60\text{--}120 M_{\odot} \text{ yr}^{-1}$, with the range representing the two different star formation contributions we estimated from the mid-IR spectral fitting. The radio detection of HDF-oMD49 with $f_{1.4 \text{ GHz}} \approx 32 \mu\text{Jy}$ (G. Morrison et al. 2008, in preparation) implies a SFR of $\approx 500 M_{\odot} \text{ yr}^{-1}$ (calculated following Bauer et al. [2002]). This is clearly inconsistent with the mid-IR data, suggesting that either the radio emission is dominated by the AGN or the radio-SFR relationship is not applicable for high-redshift objects such as HDF-oMD49.

3.2. The Chandra SED

The contrast between the weak X-ray emission (see § 2.2) and the bright, AGN-dominated IR SED implies that the AGN in HDF-oMD49 is heavily absorbed at X-ray energies. The signature of absorption should be evident in the X-ray spectrum of HDF-oMD49. However, before examining the X-ray data it is necessary to consider the contribution to the X-ray emission from star formation. Assuming a SFR of $120 M_{\odot} \text{ yr}^{-1}$ (see § 3.1) and the empirically determined L_{X} -SFR relationship found by Bauer et al. (2002), we predict a rest-frame 0.5–8 keV flux of $2 \times 10^{-17} \text{ ergs s}^{-1} \text{ cm}^{-2}$, which corresponds to an observed-frame 0.5–2 keV flux of $1.1 \times 10^{-17} \text{ ergs s}^{-1} \text{ cm}^{-2}$ ($L_{\text{X}} \approx 4 \times 10^{41} \text{ ergs s}^{-1}$), for a typical X-ray spectral slope for star-forming galaxies of $\Gamma = 1.8$. Consistent X-ray luminosities are obtained from the empirically derived Ranalli et al. (2003) relationship, although the Persic et al. (2004) relationship would predict an ≈ 4 times lower X-ray luminosity but only takes into account the contribution from high-mass X-ray binaries. These analyses show that the contribution from star formation could be significant to the observed-frame 0.5–2 keV flux ($\approx 40\%$). However, the contribution will be negligible in the other X-ray band in which HDF-oMD49 is detected (observed frame 4–8 keV).

In Figure 3 we show the X-ray data of HDF-oMD49 and compare them to the AGN model SEDs adopted by Gilli et al. (2007) to interpret the XRB. The X-ray data of HDF-oMD49 clearly indicate that the AGN is absorbed at X-ray energies; on the basis of the X-ray band ratio (see § 2.2), the X-ray data are consistent with $N_{\text{H}} > 10^{23} \text{ cm}^{-2}$ (e.g., see Fig. 4 of Alexander et al. [2003a]). However, with our low S/N X-ray data we cannot unambiguously distinguish between Compton-thick and Compton-thin absorption. Furthermore, the X-ray spectrum of a Compton-thick AGN is source specific and depends on the strength of the reflected and scattered X-ray components, in addition to the underlying power-law continuum and any additional absorption; for example, see Appendix A of Guainazzi et al. (2005) for information on the difficulty of identifying Compton-thick AGNs on the basis of X-ray colors alone. Therefore, without detailed X-ray spectral signatures that clearly indicate the presence of Compton-thick absorption (e.g., the identification of a prominent Fe K emission line or a strong reflection component), it is not possible to argue *solely* on the basis of low S/N X-ray data that an AGN is absorbed by Compton-thick material. In order to confirm whether such an X-ray-weak source is Compton thick, it is necessary to estimate the intrinsic AGN luminosity.

3.3. Quantifying the Intrinsic Properties of the AGN in HDF-oMD49

A good proxy for the intrinsic luminosity of AGN activity is the rest-frame mid-IR emission, which can provide an absorption-independent measure of the intrinsic luminosity even in the presence of Compton-thick absorption (e.g., Krabbe et al. 2001; Lutz et al. 2004; Maiolino et al. 2007; Horst et al. 2008). When

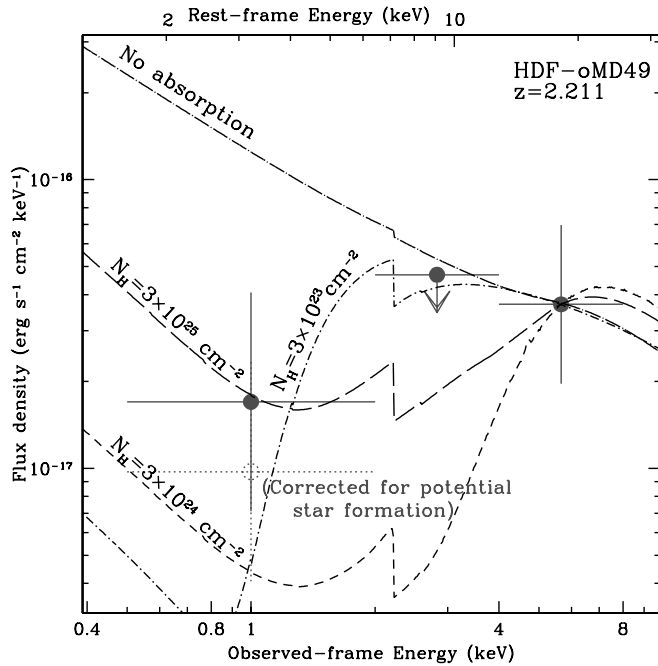


FIG. 3.— X-ray data of HDF-oMD49, compared to the AGN model SEDs adopted by Gilli et al. (2007) to interpret the XRB (model N_{H} indicated) and normalized to the observed-frame 4–8 keV flux. The open circle shows the X-ray emission at observed frame 0.5–2 keV corrected for the potential contribution from star formation; see § 3.2. The X-ray data of HDF-oMD49 are consistent with those expected for a heavily absorbed AGN; however, the low S/N X-ray spectrum alone provides limited diagnostics to distinguish between Compton-thin and Compton-thick absorption. We stress that since the data in this figure are normalized to the observed 4–8 keV flux, they do not demonstrate the >1 order-of-magnitude difference in flux between similarly powerful Compton-thin and Compton-thick AGNs; see Fig. 4. [See the electronic edition of the *Journal* for a color version of this figure.]

combined with the observed X-ray emission, the rest-frame mid-IR luminosity can therefore provide a diagnostic for the presence of heavy absorption. In this study we adopt the X-ray–6 μm luminosity relationship found by Lutz et al. (2004), which was determined by constraining the AGN continuum component in large-aperture mid-IR spectra for a sample of nearby AGNs. We favor the Lutz et al. (2004) X-ray–mid-IR luminosity relationship over the small-aperture mid-IR imaging studies of Krabbe et al. (2001) and Horst et al. (2008), since HDF-oMD49 is unresolved by *Spitzer*. Furthermore, the Lutz et al. (2004) study also covers a broader range in luminosity, and includes AGNs as luminous as those explored here. Indeed, we note that the X-ray–mid-IR luminosity ratio found for X-ray-obscured but Compton-thin quasars (Sturm et al. 2006) is consistent with the Lutz et al. (2004) relationship, indicating that it is applicable for the objects explored in our study; see Figure 4. However, the differences in the X-ray–mid-IR luminosity of these studies are small (the Lutz et al. [2004] luminosity ratio is within a factor of ≈ 2 –3 of that found by Krabbe et al. [2001] and Horst et al. [2008], assuming typical SEDs [i.e., NGC 1068; Mrk 231; M82] when converting to a common rest-frame wavelength of 6 μm).

Since it is now well established that the X-ray–to–optical luminosity ratio of optically selected AGNs is luminosity dependent (e.g., Vignali et al. 2003; Steffen et al. 2006), it is also interesting to explore whether the X-ray–mid-IR luminosity ratio is luminosity dependent. Krabbe et al. (2001), Lutz et al. (2004), and Horst et al. (2008) did not find evidence for a luminosity-dependent X-ray–mid-IR luminosity ratio for local AGNs over ≈ 3 –5 orders

of magnitude in luminosity. By comparison, the inference from the study of distant optically selected quasars by Maiolino et al. (2007) is that the X-ray–mid-IR luminosity ratio *may* be luminosity dependent. For example, solving equations (1) and (5) in Maiolino et al. (2007) gives an X-ray–mid-IR luminosity relationship of $L_{\text{X}} \propto L_{6.7\mu\text{m}}^{0.88}$. However, there is considerable uncertainty in this result, and the derived X-ray–mid-IR luminosity relationship would be linear if a different X-ray–optical luminosity ratio from Steffen et al. (2006) is used (i.e., if their eq. [1b] is adopted instead of eq. [1c]). In any case, the differences between the Lutz et al. (2004) and Maiolino et al. (2007) relationships are small (factor of <2 –3) for the luminosities of the majority of the AGNs explored here ($L_{\text{X}} < 3 \times 10^{44}$ ergs s^{-1} ; see Fig. 4); however, we indicate the cases where our results would significantly change if the luminosity-dependent version of the Maiolino et al. (2007) X-ray–mid-IR luminosity relationship is used.

In Figure 4 we show the rest-frame 2–10 keV luminosity versus 6 μm continuum luminosity of HDF-oMD49 and compare it to those found for AGNs in the local universe; we converted the rest-frame 6.7 μm data used by Maiolino et al. (2007) to rest frame 6 μm assuming the SED of NGC 1068, which results in small corrections ($\approx 10\%$). The rest-frame 2–10 keV luminosity of HDF-oMD49 ($L_{\text{X}} = 1.4 \times 10^{42}$ ergs s^{-1}) is estimated from the observed-frame 0.5–2 keV luminosity (rest frame 1.6–6.4 keV), for a spectral slope of $\Gamma = 1.4$. Assuming both the X-ray–mid-IR luminosity relationship found for local AGNs (Lutz et al. 2004), and the relationship derived from Maiolino et al. (2007), the intrinsic rest-frame 2–10 keV luminosity of HDF-oMD49 is $>10^{44}$ ergs s^{-1} , suggesting that the X-ray absorption toward the AGN in HDF-oMD49 is Compton thick; see Figure 4 and Table 1. However, to reduce further uncertainties on the X-ray–IR luminosity relationship due to, for example, the geometry and covering factor of the gas and dust surrounding the X-ray-emitting region, it is useful to have other measurements of the intrinsic AGN luminosity.

The rest-frame UV spectrum of HDF-oMD49 shows strong AGN emission lines (C IV, C III], He II, Ly α ; see Fig. 2 of Steidel et al. [2002]), which can be used to provide additional estimates of the intrinsic AGN luminosity. We calculated the emission-line fluxes using the Steidel et al. (2002) optical spectrum and integrating the flux over the emission-line profiles; see Reddy et al. (2006) for more details. Adopting the average emission-line ratios of Netzer et al. (2006), to calculate the expected [O III] $\lambda 5007$ luminosity, and the [O III] $\lambda 5007$ –X-ray flux ratio found by Mulchaey et al. (1994), the range of predicted intrinsic rest-frame 2–10 keV luminosity from the different emission lines is $(1.8$ – $4.8) \times 10^{44}$ ergs s^{-1} . We get similar intrinsic X-ray luminosities if we use the [O III] $\lambda 5007$ –X-ray flux ratio found by Alonso-Herrero et al. (1997), and we get higher intrinsic X-ray luminosities (up to an order of magnitude higher for the most luminous AGNs) if we use the Netzer et al. (2006) [O III] $\lambda 5007$ –X-ray flux ratio. We have not corrected these emission-line fluxes for extinction or contamination from star formation, which are poorly constrained at rest-frame UV wavelengths. However, we note that the Mulchaey et al. (1994), Alonso-Herrero et al. (1997), and Netzer et al. (2006) correlations were also derived using uncorrected emission-line fluxes. The uncertainties in both the emission-line ratios and the [O III] $\lambda 5007$ –X-ray flux ratio are ≈ 2 (see Table 1 of Netzer et al. [2006] and Table 2 of Mulchaey et al. [1994]), giving a combined uncertainty of a factor of ≈ 3 , comparable to the uncertainty in the intrinsic X-ray luminosity based on the rest-frame 6 μm luminosity. The intrinsic rest-frame 2–10 keV luminosities predicted from both the optical and the mid-IR spectroscopy are in good agreement, providing compelling

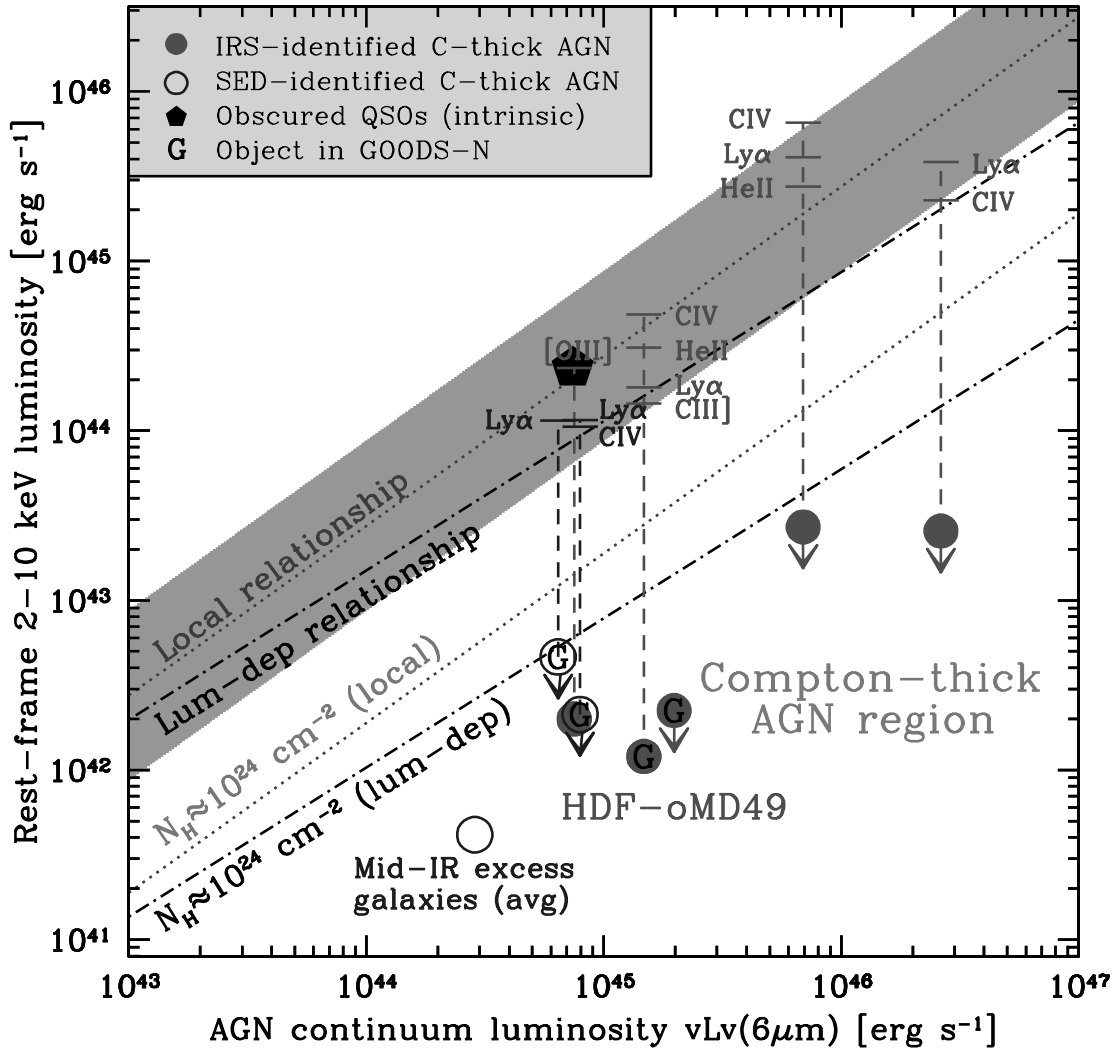


FIG. 4.—Rest-frame 2–10 keV luminosity vs. $6\ \mu\text{m}$ AGN continuum luminosity. The observed and intrinsic properties of the $z \approx 2$ AGNs selected from our study are shown; the X-ray data are converted from the observed-frame 0.5–2 keV band to the rest-frame 2–10 keV band assuming $\Gamma = 1.4$. Five of the objects are identified using *Spitzer* IRS and *Chandra* data (filled circles), and two are identified using *Spitzer* photometry and *Chandra* data (open circles); see Table 1. Objects indicated with a “G” lie in the GOODS-N field. The pentagon shows the intrinsic X-ray– $6\ \mu\text{m}$ luminosity ratio of the X-ray-obscured quasars studied by Sturm et al. (2006). The shaded region shows the range of intrinsic X-ray–mid-IR luminosity ratios found for AGNs in the local universe (taken from Lutz et al. [2004]), and the dotted lines indicate the observed rest-frame 2–10 keV– $6\ \mu\text{m}$ luminosity ratio expected for a typical AGN that is absorbed by $N_{\text{H}} \approx 10^{24}\ \text{cm}^{-2}$ (using the model presented in Alexander et al. [2005a]); the dash-dotted region shows the relationship that would be predicted assuming the luminosity-dependent $L_{\text{X}}-L_{\text{mid-IR}}$ relationship of Maiolino et al. (2007). All of the plotted AGNs lie below the track for $N_{\text{H}} \approx 10^{24}\ \text{cm}^{-2}$, suggesting that they are Compton thick. The dashed lines indicate the intrinsic 2–10 keV luminosities estimated from optical/near-IR spectroscopy (the individual emission-line luminosities are labeled) and provide good agreement with the intrinsic luminosities predicted from the mid-IR spectroscopy, confirming that all of the plotted AGNs are Compton thick. The average observed X-ray–IR luminosity ratio found for the mid-IR excess galaxies explored by Daddi et al. (2007b; open circles) is also shown, indicating that their average properties are consistent with those expected for Compton-thick AGNs about an order of magnitude less luminous than those explored here (assuming 100% of their objects are Compton-thick AGNs; see § 4.4 for discussion); however, spectroscopic observations of individual objects (some of which are presented here) are required to provide robust confirmation of Compton-thick AGN activity. [See the electronic edition of the *Journal* for a color version of this figure.]

evidence for Compton-thick absorption of an intrinsically luminous quasar in HDF-oMD49 ($L_{2-10\ \text{keV}} \approx 3 \times 10^{44}\ \text{ergs s}^{-1}$; $N_{\text{H}} \gg 10^{24}\ \text{cm}^{-2}$).

An alternative scenario for the weak X-ray emission from HDF-oMD49 is that the AGN has recently faded (e.g., Guainazzi et al. 1998). However, since the light crossing time of the mid-IR-emitting region is likely to be short (i.e., on the basis of the dust sublimation radius it will be $\approx 1-2$ yr; e.g., see Table 1 of Granato et al. [1997] and Fig. 30 of Suganuma et al. [2006]), this scenario is only tenable for HDF-oMD49 if we have caught the AGN during a very brief transitional stage where the X-ray emission has faded but the mid-IR emission is still strong. The good agreement between the fluxes measured from the *Spitzer* MIPS photometry

and the *Spitzer* IRS spectroscopy, taken 2 years apart, suggests that this scenario is unlikely.

4. DISCUSSION

We have used *Spitzer* IRS spectroscopy, 3.6–70 μm photometry, optical spectroscopy, and ultradeep 2 Ms *Chandra* data to show that HDF-oMD49 hosts an intrinsically luminous AGN that is heavily obscured by Compton-thick material ($L_{2-10\ \text{keV}} \approx 3 \times 10^{44}\ \text{ergs s}^{-1}$; $N_{\text{H}} \gg 10^{24}\ \text{cm}^{-2}$); i.e., it is a Compton-thick quasar. The S/N of the X-ray data alone was too poor to show conclusively that the AGN is obscured by Compton-thick material. However, when combined with rest-frame $6\ \mu\text{m}$ and optical emission-line luminosity constraints, the evidence for Compton-thick absorption

TABLE 1
ROBUSTLY IDENTIFIED $z \approx 2$ COMPTON-THICK QUASARS

Name	z	d_L (Mpc)	$L_{X, \text{obs}}$ (ergs s $^{-1}$)	$\nu L_{6 \mu\text{m}}$ (ergs s $^{-1}$)	$L_{\text{Ly}\alpha}$ (ergs s $^{-1}$)	$L_{\text{C IV}}$ (ergs s $^{-1}$)	$L_{\text{He II}}$ (ergs s $^{-1}$)	$L_{\text{C III}}$ (ergs s $^{-1}$)	$L_{[\text{O III}]}$ (ergs s $^{-1}$)	$L_{X, 6 \mu\text{m}}$ (ergs s $^{-1}$)	$L_{X, \text{lines}}$ (ergs s $^{-1}$)	References
SMM J123600+621047 ^a	2.002	15,750	<42.4	45.3 ^b	44.7	...	1, 2
HDF-oMD49 ^a	2.211	17,800	42.1	45.2 ^b	42.5	42.4	41.9	41.7	...	44.6	44.4	3, 4
FSC 10214+4724 ^c	2.285	18,550	42.3	44.9 ^b	42.6	44.3	44.4	5, 6, 7
SW J104406+583954	2.430	19,990	<43.4	45.8 ^b	43.9	43.5	42.9	45.2	45.6	8, 9
BX 160 ^a	2.462	20,290	<42.3	44.9 ^d	42.3	41.8	44.3	44.1	3, 4
BX 1637 ^a	2.487	20,570	<42.7	44.8 ^d	42.3	44.3	44.1	3, 4
SW J104409+585224	2.540	21,100	<43.4	46.4 ^b	43.8	43.1	45.9	45.5	8, 10

NOTES.—The luminosities are given in logarithmic units of ergs s $^{-1}$. The X-ray luminosities are given in the rest-frame 2–10 keV band: $L_{X, \text{obs}}$ is the observed X-ray luminosity calculated from the observed-frame 0.5–2 keV luminosity assuming $\Gamma = 1.4$, $L_{X, 6 \mu\text{m}}$ is the X-ray luminosity implied from the rest-frame 6 μm AGN continuum, and $L_{X, \text{lines}}$ is the average X-ray luminosity implied from the emission-line luminosities; see §§ 3.3 and 4.1 for more details. The references correspond to the X-ray, mid-IR, and optical emission-line data.

^a Object lies in the GOODS-N field.

^b Rest-frame 6 μm luminosity is calculated from the best-fitting AGN component to the *Spitzer* IRS data.

^c Data have been corrected for an assumed lensing boost of 50.

^d Rest-frame 6 μm luminosity is calculated from the *Spitzer* SED.

REFERENCES.—(1) Alexander et al. 2005a; (2) Pope et al. 2008; (3) This paper; (4) Reddy et al. 2006; (5) Alexander et al. 2005b; (6) Teplitz et al. 2006; (7) Serjeant et al. 1998; (8) Polletta et al. 2006; (9) Weedman et al. 2006; (10) Polletta et al. 2008.

in this X-ray-faint source is compelling. Additional support for this interpretation comes from the similarity to the mid-IR spectrum of HDF-oMD49 and the composite mid-IR spectrum of X-ray-obscured but Compton-thin quasars; see Figure 1*b*.

On the basis of the comparatively weak ultrahard 4–8 keV emission from HDF-oMD49, even the rest-frame 12.8–25.7 keV emission appears to be heavily suppressed. For example, assuming an X-ray spectral slope of $\Gamma = 2.0$, the predicted 12.8–25.7 keV luminosity based on the intrinsic rest-frame 2–10 keV luminosity is a factor of ≈ 20 higher than the observed 12.8–25.7 keV luminosity ($\approx 1.3 \times 10^{44}$ vs. $\approx 6 \times 10^{42}$ ergs s^{-1} ; see § 2.2). It is difficult to relate this factor of ≈ 20 suppression to an accurate estimate of the absorbing column density, since the observed X-ray emission in the 12.8–25.7 keV band could be dominated by reflected and scattered components (e.g., NGC 1068; Matt et al. 1997; see Fig. 8.1 in Comastri [2004]). However, on the basis of the PLCABS model (Yaqoob 1997) in XSPEC, which considers the effects of electron scattering and photoelectric absorption through an absorbing medium, this amount of suppression in the 12.8–25.7 keV band would correspond to an absorbing column density of $N_{\text{H}} \approx 4 \times 10^{24}$ cm^{-2} . Due to the absence of a reflection component in this model, and the simplifying assumption of a spherical geometry, this absorbing column density should only be considered representative (e.g., see Fig. 8.1 in Comastri [2004] for an alternative model).

In this final section we adopt the approach that we used in § 3 to identify other distant Compton-thick AGNs using data obtained from the literature. Utilizing these constraints we then directly estimate the space density of Compton-thick quasars at $z \approx 2$ and compare our results to current observational and theoretical constraints.

4.1. The Identification of Other Distant Compton-thick AGNs

From a search of the published *Spitzer* IRS spectroscopic data, there are four good candidate $z \approx 2$ Compton-thick AGNs that have mid-IR spectroscopy and the *essential* sensitive X-ray constraints required to identify Compton-thick AGN activity: FSC 10214+4714, SW J104406+583954, SW J104409+585224, and SMM J123600+621047.

FSC 10214+4714 is a strongly lensed Seyfert 2 galaxy at $z = 2.285$ which produces luminous 6 μm AGN continuum emission (Teplitz et al. 2006) but is only weakly detected at X-ray energies, despite an effective lensing-corrected *Chandra* exposure of ≈ 2 Ms (Alexander et al. 2005b). In Figure 4 we plot FSC 10214 and provide secondary support for the intrinsic luminosity of the AGN using the [O III] $\lambda 5007$ luminosity from Alexander et al. (2005b) and the [O III] $\lambda 5007$ –X-ray flux ratio of Mulchaey et al. (1994); see Table 1. The combination of the X-ray data and optical–mid-IR spectroscopy confirms that FSC 10214 hosts a Compton-thick quasar ($L_{2-10\text{keV}} \approx 2 \times 10^{44}$ ergs s^{-1}), even given the considerable scatter in the relationships.

SW J104406+583954 and SW J104409+585224 are X-ray-weak candidate Compton-thick AGNs identified in the *Chandra*/SWIRE (*Spitzer* Wide-Area Infrared Extragalactic) survey (Polletta et al. 2006) that lie at $z = 2.430$ and $z = 2.540$, respectively. The optical and mid-IR spectra of both sources show clear signatures of AGN activity (Polletta et al. 2006, 2008; Weedman et al. 2006), which we use to determine the intrinsic luminosities of the central sources; see Table 1. In Figure 4 we plot their X-ray–6 μm luminosities, showing that the properties of both objects are consistent with those expected for a luminous Compton-thick quasar ($L_{2-10\text{keV}} > 10^{45}$ ergs s^{-1}); however, we note that the evidence is weaker for SW 104406 if the luminosity-dependent X-ray–

to–mid-IR luminosity relationship inferred from Maiolino et al. (2007) is used.

SMM J123600+621047 is a $z = 2.002$ submillimeter-emitting galaxy (SMG) with a mid-IR-bright AGN (Pope et al. 2008) that is undetected in the 2 Ms CDF-N data (Alexander et al. 2003b); we ran WAVDETECT using a false-positive probability threshold of 10^{-5} but did not detect X-ray emission from this source (see Table 1 of Alexander et al. [2005a]). The X-ray–6 μm luminosity ratio indicates that it hosts a Compton-thick AGN (see Fig. 4), although optical and near-IR spectroscopic observations do not reveal the signatures of AGN activity (e.g., Swinbank et al. 2004; Chapman et al. 2005), leaving some uncertainty on the intrinsic luminosity of the AGN. However, since the mid-IR luminosity of the AGN in SMMJ 123600 is about an order of magnitude larger than that found in typical SMGs (e.g., Lutz et al. 2005; Menéndez-Delmestre et al. 2007; Valiante et al. 2007; Pope et al. 2008), the ≈ 10 times larger intrinsic X-ray luminosity derived here seems plausible ($L_{\text{X},6\mu\text{m}} \approx 5 \times 10^{44}$ ergs s^{-1} ; i.e., compare to Alexander et al. 2005a); see our Table 1. In Alexander et al. (2005c), it was argued that SMGs represent a rapid black hole growth phase before the onset of optically luminous quasar activity. The discovery of this one mid-IR luminous X-ray-undetected SMG in the CDF-N field increases current constraints on the *integrated* black hole growth density in SMGs by a factor of ≈ 2 (see Fig. 2 of Alexander et al. [2005c]).

Other studies have used optical spectroscopy to identify AGNs that are mid-IR bright and X-ray weak/undetected but lack *Spitzer* IRS spectroscopy. Reddy et al. (2006) found two $z \approx 2.4$ – 2.5 optically identified AGNs (BX 160; BX 1637) that are X-ray undetected in the 2 Ms CDF-N survey and have power-law-like IR SEDs [the 24 μm fluxes of these sources ($f_{24\mu\text{m}} \approx 100$ – 140 μJy) are too faint for good S/N *Spitzer* IRS spectroscopy]; see Table 1. Following our approach for HDF-oMD49 (see § 2.2), we ran WAVDETECT using a false-positive probability threshold of 10^{-5} but did not detect X-ray emission from either source; 3σ X-ray upper limits are calculated following § 3.4.1 in Alexander et al. (2003b). We plot the X-ray–to–6 μm luminosity ratios of these objects in Figure 4. The mid-IR data, when combined with the optical emission-line luminosities, indicate that these sources are likely to be Compton-thick quasars; we determined their emission-line properties using the same procedure as for HDF-oMD49 (see § 3.3). The evidence would be weaker for BX 1637 if the luminosity-dependent X-ray–mid-IR luminosity ratio inferred from Maiolino et al. (2007) is used, although we note that the X-ray–6 μm luminosity ratio for this source is an upper limit.

We also note that other studies have selected candidate Compton-thick AGNs using a combination of multiwavelength data with sensitive X-ray constraints (e.g., Donley et al. 2005, 2007; Alonso-Herrero et al. 2006; Daddi et al. 2007b; Martínez-Sansigre et al. 2007; Fiore et al. 2008); many other studies have identified obscured AGNs using mid-IR spectroscopy but lack the *essential* X-ray data to provide a case for Compton-thick absorption. However, none of these studies have optical or mid-IR spectroscopy to provide accurate measurements of the intrinsic AGN luminosities.

4.2. The Properties of Distant Compton-thick AGNs

The intrinsic X-ray–mid-IR continuum ratios, inferred using the rest-frame UV emission-line luminosities of the six Compton-thick quasars with optical AGN signatures, are consistent with those found for AGNs in the local universe; see Figure 4. This is in agreement with the results of Sturm et al. (2006), who found that the *average* intrinsic X-ray–6 μm luminosities of distant X-ray-obscured quasars are similar to those found for local AGNs,

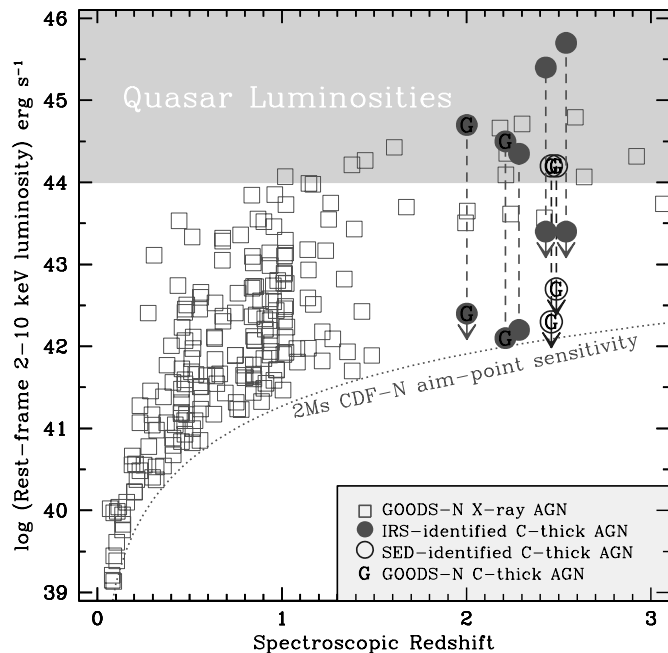


FIG. 5.—Rest-frame 2–10 keV luminosity vs. spectroscopic redshift for the X-ray-detected sources in the GOODS-N region of the CDF-N survey and the seven Compton-thick AGNs identified here; the four Compton-thick AGNs that lie in the GOODS-N field are indicated with a “G.” The dotted curve shows the aim-point sensitivity limit for the CDF-N survey; see Fig. 18 of Alexander et al. (2003b) for the drop in *Chandra* sensitivity for off-axis sources. The source redshifts are predominantly taken from Barger et al. (2003). The dashed lines connect the observed X-ray luminosity of the Compton-thick AGNs to their intrinsic luminosities; the intrinsic luminosities correspond to the mean luminosity estimated from the combination of the $6\ \mu\text{m}$ luminosity and the average emission-line luminosity given in Table 1. Although the four Compton-thick AGNs that lie in the GOODS-N region are either X-ray weak or undetected, they are among the most intrinsically luminous AGNs in the GOODS-N field. [See the electronic edition of the Journal for a color version of this figure.]

suggesting that the objects explored here are the extreme Compton-thick end of the X-ray-obscured quasar population. We also showed in § 3.1 and Figure 1b that the *Spitzer* IRS spectrum of HDF-oMD49 is similar to the composite mid-IR spectrum produced by Sturm et al. (2006), providing a particularly strong case for a quasar that is absorbed in the X-ray band by Compton-thick material in this source. These pieces of evidence also suggest that the accretion properties of distant, optically identifiable AGNs are similar to those observed in local AGNs, in agreement with previous studies that have explored the X-ray–optical and X-ray–infrared properties of optically selected AGNs (e.g., Steffen et al. 2006; Jiang et al. 2006).

In Figure 5 we show the observed and intrinsic X-ray luminosities versus redshift of the seven Compton-thick quasars identified here. Four of the Compton-thick quasars lie in the GOODS-N region ($\approx 160\ \text{arcmin}^2$) of the CDF-N and, despite being X-ray weak/undetected, they are among the most intrinsically luminous AGNs identified in this field. This shows that even in the deepest X-ray survey currently available, we are only able to directly probe the peak of the Compton-thick AGN population at $z \approx 2$. The two luminous Compton-thick quasars were identified in the wider area SWIRE survey ($\approx 0.6\ \text{deg}^2$) and are among the most luminous obscured AGNs known.

Four of the seven Compton-thick quasars are detected in the X-ray band, most typically at $>2\ \text{keV}$. Three of these objects have hard X-ray spectra ($\Gamma < 1$; HDF-oMD49; SW 104406; SW 104409; Polletta et al. 2006), and one object has a comparatively soft X-ray spectrum ($\Gamma \approx 1.6$; FSC 10214; Alexander et al. 2005c). The

comparatively soft X-ray spectrum of FSC 10214 might be dominated by scattered emission and star formation from the host galaxy, as often found in Compton-thick AGNs (e.g., Bassani et al. 1999; Comastri 2004; Guainazzi et al. 2005). We can also place basic X-ray spectral constraints on the three X-ray-undetected Compton-thick quasars by stacking their X-ray data; all of these objects lie in the GOODS-N field, where the X-ray data are particularly sensitive. Using the X-ray stacking code adopted by Worsley et al. (2005), we obtain $\approx 3\ \sigma$ detections in the 0.5–8 and 2–8 keV bands, and have a $\approx 2\ \sigma$ constraint in the 0.5–2 keV band; the significance of these stacking results were calculated using 10,000 Monte Carlo trials. The stacked data correspond to fluxes (and a $3\ \sigma$ upper limit) of $2.8 \times 10^{-16}\ \text{ergs s}^{-1}\ \text{cm}^{-2}$ (0.5–8 keV), $< 2.3 \times 10^{-17}\ \text{ergs s}^{-1}\ \text{cm}^{-2}$ (0.5–2 keV), and $2.7 \times 10^{-16}\ \text{ergs s}^{-1}\ \text{cm}^{-2}$ (2–8 keV). The average rest-frame 2–10 keV luminosity constraint for these three objects derived from the observed-frame 0.5–2 keV flux is $< 10^{42}\ \text{ergs s}^{-1}$. The derived X-ray spectral slope of $\Gamma < 0.3$ unambiguously confirms that heavily obscured AGNs are present in these sources (e.g., see Fig. 2a in Alexander et al. [2005a]).

4.3. The Selection of Distant Compton-thick AGNs

The seven Compton-thick quasars investigated here were selected on the basis of unambiguous evidence for AGN activity from optical and/or mid-IR spectroscopy. The advantage with this approach is that we have been able to estimate the intrinsic AGN properties of these objects using the optical–mid-IR spectroscopy. However, the requirement for spectroscopic evidence of AGN activity has led to a comparatively small sample of objects. Nevertheless, we can provide some insight into the completeness of Compton-thick AGN selection by comparing the properties of our reliably identified Compton-thick quasars to the larger samples of candidate Compton-thick AGNs that have been photometrically identified in other studies. Arguably, the most complete identification studies of distant Compton-thick AGNs to date are Daddi et al. (2007a, 2007b) and Fiore et al. (2008).

Daddi et al. (2007a, 2007b) identified a large population of X-ray-undetected $z \approx 2$ galaxies with an excess of mid-IR emission over that expected from star formation (as predicted using the dust-extinction-corrected UV luminosity). X-ray stacking analyses revealed a hard X-ray spectral slope from these objects ($\Gamma = 0.8$), comparable to that of the Compton-thick quasars and unambiguously identifying the presence of heavily obscured AGNs; see § 4.2. In Figure 6a we plot the ratio of mid-IR-based to UV-based SFR versus $8\ \mu\text{m}$ luminosity of the Compton-thick quasars and compare them to Daddi et al. (2007a, 2007b); we have not calculated the properties of FSC 10214 due to the significant uncertainties in the lensing magnification of the star-forming regions. The Compton-thick quasars lie significantly above the mid-IR excess threshold defined by Daddi et al. (2007b), indicating that they are extreme examples of the mid-IR excess galaxy population. This analysis shows reliably that at least a subsample of the mid-IR excess galaxy population host Compton-thick AGNs.

Fiore et al. (2008) took a complementary approach to that of Daddi et al. (2007a, 2007b) and selected X-ray-undetected objects with extreme mid-IR–to–optical flux ratios ($f_{24\ \mu\text{m}}/f_R > 1000$) and red optical colors ($R - K > 4.5$). X-ray stacking analyses of these objects revealed a hard X-ray spectrum with a slope similar to that found for the mid-IR excess galaxies ($\Gamma \approx 1.0$, calculated from their stacked X-ray count rates). In Figure 6b we plot the mid-IR–to–optical flux ratio versus $R - K$ color of the Compton-thick quasars and compare them to the candidate Compton-thick AGNs studied by Fiore et al. (2008) and Daddi et al. (2007b); as before, we did not calculate the properties of FSC 10214. Formally,

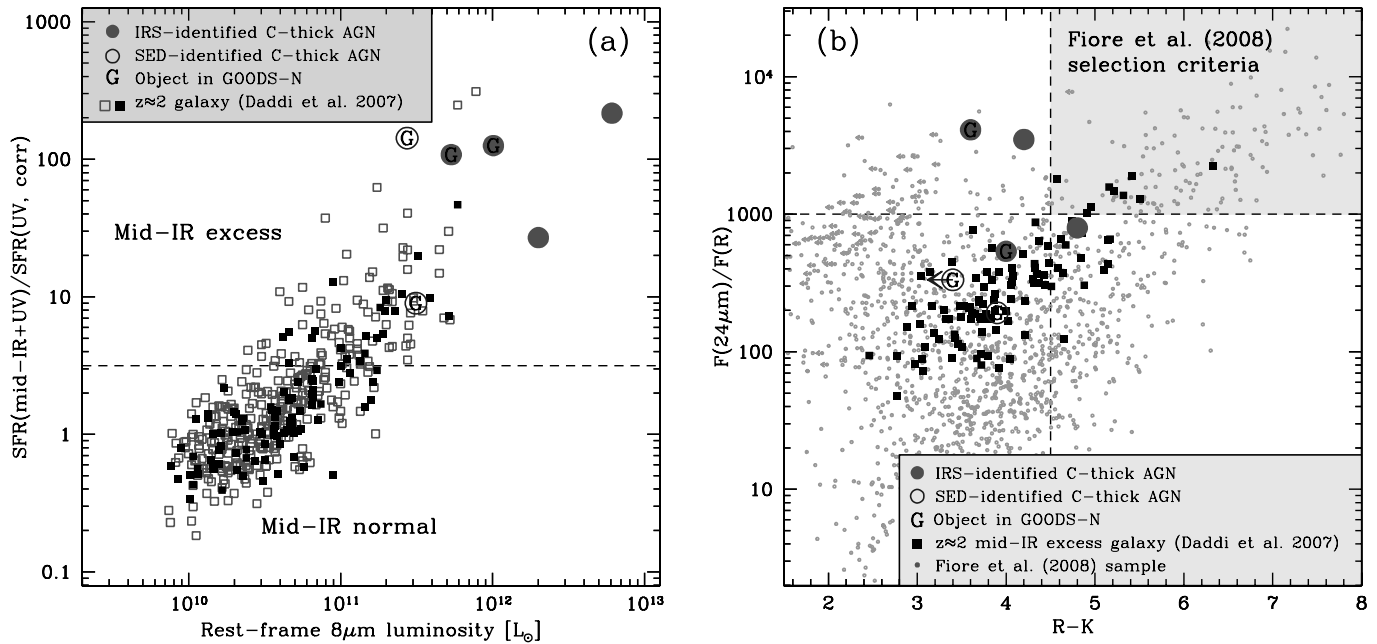


FIG. 6.— Selection of distant Compton-thick AGNs. (a) Ratio of mid-IR-based to UV-based SFR vs. $8\mu\text{m}$ luminosity for the $z \approx 2$ galaxies studied by Daddi et al. (2007a, 2007b) and the spectroscopically identified Compton-thick quasars; the open and filled symbols correspond to objects with photometric and spectroscopic redshifts, respectively. This figure has been adapted from Fig. 2 of Daddi et al. (2007b). (b) Mid-IR–optical flux ratio vs. $R - K$ color for the galaxies investigated by Fiore et al. (2008) and Daddi et al. (2007a, 2007b) and the spectroscopically identified Compton-thick quasars; see also Fig. 3 of Fiore et al. (2008). FSC 10214+4724 is not plotted on these figures, since there is some uncertainty on the lensing magnification of the star-forming component. The dashed lines indicate the selection criteria for the Daddi et al. (2007b) and Fiore et al. (2008) studies. Our spectroscopically identified Compton-thick quasars are extreme examples of the mid-IR excess galaxy population of Daddi et al. (2007b), but none of them formally match the Fiore et al. (2008) selection criteria, which is probably due to the requirement for an optical signature of AGN activity in our sample. This implies that there could be many more distant Compton-thick AGNs than that suggested by either study alone. [See the electronic edition of the *Journal* for a color version of this figure.]

none of the Compton-thick quasars match the candidate Compton-thick AGN selection criteria of Fiore et al. (2008), although two of the objects lie close. Furthermore, only $\approx 10\%$ of the mid-IR excess galaxies of Daddi et al. (2007b) match the Fiore et al. (2008) criteria. These analyses show that the candidate Compton-thick AGN criteria of Daddi et al. (2007b) and Fiore et al. (2008) are mutually exclusive, suggesting that the distant X-ray-undetected AGN population may be larger than either study has suggested. The requirement in our study for optical spectroscopic redshifts and the optical identification of AGN activity (with the exception of SMM J123600) probably causes a bias against selecting objects with red $R - K$ colors, which by definition will be optically faint.

4.4. The Ubiquity of Distant Compton-thick AGNs

Our seven Compton-thick quasars do not comprise a complete sample. However, four of the objects lie in the GOODS-N field, providing basic constraints on the space density of Compton-thick quasars at $z \approx 2-2.5$. On the basis of the comoving volume at $z = 2-2.5$ in a region the size of the GOODS-N field, we estimate a comoving space density for Compton-thick quasars with $L_{2-10\text{keV}} \approx 10^{44}-10^{45}\text{ergs s}^{-1}$ of $\Phi \approx (0.7-2.5) \times 10^{-5}\text{Mpc}^{-3}$, where the range only reflects the uncertainty due to small number statistics (e.g., Gehrels 1986).

In Figure 7 we plot the Compton-thick quasar space density and compare it to that found in other studies. Our results suggest that the space density of Compton-thick quasars is $\approx 1-5$ times higher than that of comparably luminous unobscured quasars at $z \approx 2-2.5$ ($\Phi \approx 5 \times 10^{-6}\text{Mpc}^{-3}$; e.g., Hasinger et al. 2005). Since the Gilli et al. (2007) model of the XRB constrains the number of Compton-thick quasars to be the same as the number of unobscured quasars, our Compton-thick quasar space density is also $\approx 1-5$ times higher than the Compton-thick quasar predic-

tions of Gilli et al. (2007). As we mention in § 4.1 and show in Figure 4, the evidence for a Compton-thick quasar in BX 1637 is weaker if the X-ray–mid-IR luminosity ratio inferred by Maiolino et al. (2007) is used. However, we note that a significantly more important issue is likely to be the effect of cosmic variance, since we have only identified Compton-thick quasars in a small region over a narrow redshift range. For example, within the GOODS-N field, there are also four X-ray-unobscured quasars that lie at $z \approx 2-2.5$, indicating that the true Compton-thick–unobscured quasar ratio may be toward the lower end of the value given above. Nevertheless, our results clearly indicate that a large fraction of the growth of black holes was obscured by Compton-thick material, in general agreement with results based on less reliable photometrically identified objects (e.g., Daddi et al. 2007b; Martínez-Sansigre et al. 2007; Fiore et al. 2008), the predictions made by theoretical models (e.g., Marconi et al. 2004; Treister et al. 2006), and the Compton-thick AGN fraction inferred by the study of Maiolino et al. (2007; their Fig. 7a).

We can compare our estimated space density to those determined from the photometric selection of candidate Compton-thick AGNs by Daddi et al. (2007b) and Fiore et al. (2008). On the basis of the X-ray data and the X-ray– $6\mu\text{m}$ luminosity, Daddi et al. (2007b) argued that their candidate Compton-thick AGNs have an average intrinsic luminosity of $L_{2-10\text{keV}} \approx (1-4) \times 10^{43}\text{ergs s}^{-1}$. The intrinsic luminosities of these mid-IR excess galaxies are about an order of magnitude lower than the Compton-thick quasars identified here, and consequently their space density is higher ($\Phi \approx 2.6 \times 10^{-4}\text{Mpc}^{-3}$; see Fig. 7). Fiore et al. (2008) estimated the intrinsic X-ray luminosities of their X-ray-undetected candidate Compton-thick AGNs using the $5.8\mu\text{m}$ luminosities, finding $L_{2-10\text{keV}} > 10^{43}\text{ergs s}^{-1}$. Taking into account the estimated redshift range of their objects ($z \approx 1.2-2.6$), we calculate a space density of $\Phi \approx 7 \times 10^{-5}\text{Mpc}^{-3}$; as mentioned in Fiore et al.

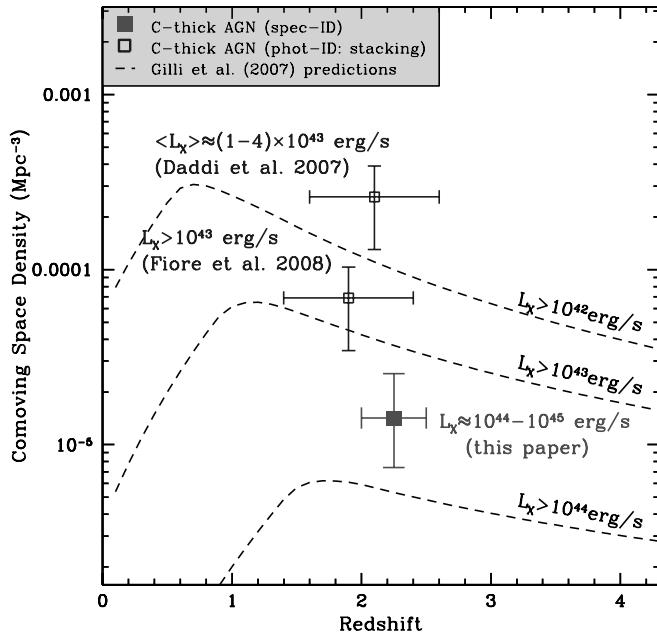


FIG. 7.— Space density of Compton-thick AGNs. The filled square corresponds to the results determined here for spectroscopically identified Compton-thick quasars with $L_{2-10\text{ keV}} \approx 10^{44}-10^{45}$ ergs s^{-1} that lie in the GOODS-N region of the CDF-N field. The open squares correspond to the results obtained by Daddi et al. (2007b) and Fiore et al. (2008) using photometrically identified objects and X-ray stacking analyses; the plotted values assume that 100% of their objects are Compton-thick AGNs, and they are therefore upper limits (see § 4.4 for discussion). The dashed lines are the predicted space densities of Compton-thick AGNs for a range of X-ray luminosity lower limits from the Gilli et al. (2007) XRB model. The space density of the Compton-thick quasars robustly identified here is a factor of $\approx 1-5$ higher than that found for comparably luminous unobscured quasars, indicating that Compton-thick accretion is ubiquitous at $z \approx 2$; see § 4.4 for a more detailed discussion. [See the electronic edition of the Journal for a color version of this figure.]

(2008), this space density is consistent with that predicted for Compton-thick AGNs using the XRB model from Gilli et al. (2007). Taken at face value, these results suggest that lower luminosity Compton-thick AGNs were $\approx 5-20$ times more common than Compton-thick quasars at $z \approx 2$. However, since the primary evidence for Compton-thick AGN activity in these studies was from X-ray stacking analyses, there could be significant numbers of non-Compton-thick AGNs in their samples (i.e., either Compton-thin AGNs or star-forming galaxies). Both Daddi et al. (2007b) and Fiore et al. (2008) assessed the “contamination” from star-forming galaxies to their stacked X-ray results and concluded that $\geq 50\%$ and $\approx 80\% \pm 15\%$ of the objects are heavily obscured AGNs, respectively. However, these percentages refer to the fraction of photometrically identified objects that are heavily obscured AGNs, and direct optical–mid-IR spectroscopic identification will be required to determine what fraction of these AGNs are obscured by Compton-thick material.

We can also compare our results to those determined for more luminous Compton-thick quasars. Polletta et al. (2006) identified five candidate Compton-thick quasars at $z \approx 1.4-2.6$ with $L_{2-10\text{ keV}} > 10^{45}$ ergs s^{-1} on the basis of the *Chandra* data in the SWIRE survey, giving a space density of $\Phi \approx 5.7 \times 10^{-7}$ Mpc $^{-3}$. Two of these objects have been presented here as robust Compton-thick quasars (SW J104406 and SW J104409; see Table 1). However, the other three candidate Compton-thick quasars are all undetected at $24\ \mu\text{m}$ ($f_{24\ \mu\text{m}} < 230\ \mu\text{Jy}$; see Table 2 of Polletta et al. [2006]). This suggests that either the intrinsic AGN luminosities of these Compton-thick quasars are more modest ($L_{2-10\text{ keV}} < 10^{45}$ ergs s^{-1}) than those estimated by Polletta et al. (2006), or that the X-ray–mid-IR relationship shown in Figure 4 does not hold

for these luminous objects. Martínez-Sansigre et al. (2007) identified 10 Compton-thick quasars at $z \approx 1.7-4.2$ with an average bolometric luminosity of $L_{\text{bol}} \approx 10^{47}$ ergs s^{-1} , giving a space density of $\Phi \approx 3.9 \times 10^{-8}$ Mpc $^{-3}$. On the basis of the bolometric conversion of Elvis et al. (1994), which Martínez-Sansigre et al. (2007) also adopted, the estimated average X-ray luminosities are $L_{2-10\text{ keV}} \approx 3 \times 10^{45}$ ergs s^{-1} for these sources, suggesting that they are very luminous AGNs. However, since two of their objects are Compton-thin quasars that are detected at X-ray energies, we can directly estimate the intrinsic 2–10 keV luminosities of the candidate Compton-thick quasars using the average X-ray–6 μm luminosity ratio of the Compton-thin quasars. Taking this approach and using the median 24 μm flux for the sample, the typical intrinsic X-ray luminosities of these quasars would be more modest ($L_{2-10\text{ keV}} \approx 3 \times 10^{44}$ ergs s^{-1}), casting significant doubt on whether they are obscured by Compton-thick material; the rest-frame 6 μm fluxes are derived from the observed 24 μm fluxes using the NGC 1068 SED to apply small K -corrections. Direct spectroscopic identification of these photometrically classified Compton-thick quasars is required to place more direct constraints, which should be possible with current instrumentation.

Finally, we compare our results to the Compton-thick AGNs identified by Tozzi et al. (2006) using X-ray spectral analysis of X-ray-detected AGNs in the *Chandra* Deep Field–South survey. Fourteen of the objects investigated by Tozzi et al. (2006) had X-ray spectra that were better fitted by a pure reflection model than an absorbed power-law model, and were consequently classified as Compton-thick AGNs; derived space densities are $\Phi \approx 3 \times 10^{-5}$ Mpc $^{-3}$ at $z \approx 1$ and $\Phi \approx 8 \times 10^{-6}$ Mpc $^{-3}$ at $z \approx 2$. While the Tozzi et al. (2006) study provides the most quantitative X-ray identification of distant Compton-thick AGNs to date, it is also possible for Compton-thin AGNs to have a pure reflection component (i.e., if the power-law component has temporarily decreased), and other pieces of evidence are required to confirm that these are Compton-thick AGNs. Two of the seven objects with spectroscopic redshifts have strong Fe $K\alpha$ emission lines, confirming that they are likely to be Compton thick, but supporting evidence for Compton-thick absorption is lacking in the other objects.

4.5. Prospects for Improved Observational Constraints

The current study provides diagnostics to identify distant Compton-thick AGNs but is limited in source statistics, covers a narrow redshift range, and is restricted to the brightest AGNs at $z \approx 2$. Future studies could focus on obtaining optical–mid-IR spectroscopy of lower luminosity $z \approx 2$ candidate Compton-thick AGNs, as well as identifying objects at lower and higher redshifts. Assuming the NGC 1068 template used here and the average X-ray–mid-IR relationship shown in Figure 4, an AGN with $L_{2-10\text{ keV}} \approx 10^{43}$ ergs s^{-1} will have 24 μm fluxes of $\approx 2\ \mu\text{Jy}$, $\approx 15\ \mu\text{Jy}$, $\approx 0.3\ \text{mJy}$, and $\approx 5\ \text{mJy}$ at $z \approx 4$, $z \approx 2$, $z \approx 0.7$, and $z \approx 0.2$, respectively; these fluxes will typically scale linearly with luminosity (see § 3.3). Mid-IR-bright objects ($f_{24\ \mu\text{m}} > 0.2\ \text{mJy}$) should be identifiable with *Spitzer* IRS, but mid-IR spectroscopic identification of fainter objects will need to wait until the launch of the *James Webb Space Telescope*. Optical and near-IR spectroscopy may be easier to obtain for many of the candidate Compton-thick AGNs, although only if the AGNs have identifiable emission lines, which could be weak in low-luminosity and dust-reddened AGNs (e.g., Caccianiga et al. 2007; see § 4.3).

Ultimately, deep X-ray data are required to search directly for the presence of Compton-thick absorption in individual objects using high S/N X-ray spectroscopy. For the majority of the objects investigated here, this will require $\gg 2$ Ms exposures with current X-ray telescopes; see Figure 5. However, due to its large

lensing boost, it is possible to provide reasonable X-ray spectral constraints for FSC 10214+4724 in a modest *Chandra* exposure (e.g., a 100 ks *Chandra* exposure would yield almost 100 X-ray counts, >10 times more than found for HDF-oMD49; see Fig. 3). Large improvements in the X-ray spectral constraints for distant Compton-thick AGNs will need to wait for the next generation of X-ray observatories (e.g., *Constellation-X*, *NuSTAR*, *Simbol-X*, and *XEUS*), where the foci are high-resolution spectroscopy and/or high-energy imaging (>10 KeV) of faint X-ray sources. For example, a 1 Ms *XEUS* exposure will yield ≈ 5000 counts for HDF-oMD49, allowing detailed X-ray spectral analyses and providing the potential to search for changes in the X-ray emission due to column density variations, giving direct insight into the environment around the black hole of a distant Compton-thick AGN (e.g., Risaliti et al. 2002).

5. CONCLUSIONS

We have presented *Spitzer* IRS spectroscopy and 3.6–70 μm photometry of HDF-oMD49, a $z = 2.211$ optically identified AGN that is formally undetected in the 2 Ms CDF-N observation. From a combination of optical–mid-IR spectroscopy and X-ray data, we have shown that HDF-oMD49 hosts an intrinsically luminous quasar that is obscured by Compton-thick material ($L_{2-10\text{ keV}} \approx 3 \times 10^{44} \text{ ergs s}^{-1}$; $N_{\text{H}} \gg 10^{24} \text{ cm}^{-2}$). We selected six further $z \approx 2$ AGNs from the literature (four with *Spitzer* IRS spectroscopy) and used the same X-ray–optical–mid-IR diagnostics applied to HDF-oMD49 to show that these objects are also likely to be Compton-thick quasars with $L_{2-10\text{ keV}} > 10^{44} \text{ ergs s}^{-1}$. We demonstrated that these Compton-thick quasars would be classified as

mid-IR excess galaxies, on the basis of the Daddi et al. (2007b) definition, providing the first spectroscopic confirmation of Compton-thick AGN activity in a subsample of these $z \approx 2$ mid-IR-bright galaxies. Four of these Compton-thick quasars lie in the GOODS-N field, and we used these objects to constrain the space density of distant Compton-thick quasars, finding $\Phi \approx (0.7-2.5) \times 10^{-5} \text{ Mpc}^{-3}$ at $z \approx 2-2.5$. On the basis of our results, Compton-thick quasars were as ubiquitous as unobscured quasars at $z \approx 2-2.5$, implying that a large fraction of the growth of supermassive black holes must have been obscured by Compton-thick material.

We acknowledge support from the Royal Society (D. M. A.), the *Spitzer Space Telescope* Fellowship program (A. P.), the Natural Sciences and Engineering Research Council of Canada and the Canadian Space Agency (A. P.), the *Chandra* Fellowship program (F. E. B.), and the NASA LTSA grant NAG5-13035 (W. N. B.). We thank R. Gilli for generously providing his model tracks and Compton-thick AGN spectra, and for his insightful comments on an earlier draft of this paper. We also thank F. Fiore for providing the data from his sample; E. Sturm for providing the composite obscured quasar spectrum; C. Done, M. Polletta, and E. Treister for scientific feedback; and the referee for useful suggestions. This work is based in part on observations made with the *Spitzer Space Telescope*, which is operated by the Jet Propulsion Laboratory, California Institute of Technology under a contract with NASA. The IRS was a collaborative venture between Cornell University and Ball Aerospace Corporation funded by NASA through the Jet Propulsion Laboratory and Ames Research Center.

REFERENCES

- Alexander, D. M., Bauer, F. E., Chapman, S. C., Smail, I., Blain, A. W., Brandt, W. N., & Ivison, R. J. 2005a, *ApJ*, 632, 736
- Alexander, D. M., Brandt, W. N., Hornschemeier, A. E., Garmire, G. P., Schneider, D. P., Bauer, F. E., & Griffiths, R. E. 2001, *AJ*, 122, 2156
- Alexander, D. M., Chartas, G., Bauer, F. E., Brandt, W. N., Simpson, C., & Vignali, C. 2005b, *MNRAS*, 357, L16
- Alexander, D. M., Smail, I., Bauer, F. E., Chapman, S. C., Blain, A. W., Brandt, W. N., & Ivison, R. J. 2005c, *Nature*, 434, 738
- Alexander, D. M., et al. 2003a, *AJ*, 125, 383
- . 2003b, *AJ*, 126, 539
- Allen, C. W. 1973, *Astrophysical Quantities* (3rd ed.; London: Univ. London, Athlone Press)
- Alonso-Herrero, A., Quillen, A. C., Rieke, G. H., Ivanov, V. D., & Efstathiou, A. 2003, *AJ*, 126, 81
- Alonso-Herrero, A., Quillen, A. C., Simpson, C., Efstathiou, A., & Ward, M. J. 2001, *AJ*, 121, 1369
- Alonso-Herrero, A., Ward, M. J., & Kotilainen, J. K. 1997, *MNRAS*, 288, 977
- Alonso-Herrero, A., et al. 2006, *ApJ*, 640, 167
- Barger, A. J., et al. 2003, *AJ*, 126, 632
- Bassani, L., Dadina, M., Maiolino, R., Salvati, M., Risaliti, G., della Ceca, R., Matt, G., & Zamorani, G. 1999, *ApJS*, 121, 473
- Bauer, F. E., Alexander, D. M., Brandt, W. N., Hornschemeier, A. E., Vignali, C., Garmire, G. P., & Schneider, D. P. 2002, *AJ*, 124, 2351
- Bauer, F. E., Alexander, D. M., Brandt, W. N., Schneider, D. P., Treister, E., Hornschemeier, A. E., & Garmire, G. P. 2004, *AJ*, 128, 2048
- Brandt, W. N., & Hasinger, G. 2005, *ARA&A*, 43, 827
- Brandt, W. N., et al. 2001, *AJ*, 122, 2810
- Caccianiga, A., Severgnini, P., Della Ceca, R., Maccacaro, T., Carrera, F. J., & Page, M. J. 2007, *A&A*, 470, 557
- Chapman, S. C., Blain, A. W., Smail, I., & Ivison, R. J. 2005, *ApJ*, 622, 772
- Chary, R., & Elbaz, D. 2001, *ApJ*, 556, 562
- Comastri, A. 2004, in *Supermassive Black Holes in the Distant Universe*, ed. A. J. Barger (Dordrecht: Kluwer), 245
- Daddi, E., et al. 2007a, *ApJ*, 670, 156
- . 2007b, *ApJ*, 670, 173
- Donley, J. L., Rieke, G. H., Pérez-González, P. G., Rigby, J. R., & Alonso-Herrero, A. 2007, *ApJ*, 660, 167
- Donley, J. L., Rieke, G. H., Rigby, J. R., & Pérez-González, P. G. 2005, *ApJ*, 634, 169
- Efstathiou, A., & Rowan-Robinson, M. 1995, *MNRAS*, 273, 649
- Elvis, M., et al. 1994, *ApJS*, 95, 1
- Fiore, F., et al. 2008, *ApJ*, 672, 94
- Frayser, D. T., et al. 2006, *ApJ*, 647, L9
- Freeman, P. E., Kashyap, V., Rosner, R., & Lamb, D. Q. 2002, *ApJS*, 138, 185
- Galliano, E., Alloin, D., Granato, G. L., & Villar-Martín, M. 2003, *A&A*, 412, 615
- Gehrels, N. 1986, *ApJ*, 303, 336
- George, I. M., & Fabian, A. C. 1991, *MNRAS*, 249, 352
- Giacconi, R., et al. 2002, *ApJS*, 139, 369
- Gilli, R., Comastri, A., & Hasinger, G. 2007, *A&A*, 463, 79
- Granato, G. L., Danese, L., & Franceschini, A. 1997, *ApJ*, 486, 147
- Guainazzi, M., Matt, G., & Perola, G. C. 2005, *A&A*, 444, 119
- Guainazzi, M., et al. 1998, *MNRAS*, 301, L1
- Hao, L., Weedman, D. W., Spoon, H. W. W., Marshall, J. A., Levenson, N. A., Elitzur, M., & Houck, J. R. 2007, *ApJ*, 655, L77
- Hasinger, G., Miyaji, T., & Schmidt, M. 2005, *A&A*, 441, 417
- Horst, H., Gandhi, P., Smette, A., & Duschl, W. J. 2008, *A&A*, 479, 389
- Houck, J. R., et al. 2004, *ApJS*, 154, 18
- Jiang, L., et al. 2006, *AJ*, 132, 2127
- Kormendy, J., & Richstone, D. 1995, *ARA&A*, 33, 581
- Krabbe, A., Böker, T., & Maiolino, R. 2001, *ApJ*, 557, 626
- Kwan, J., & Krolik, J. H. 1981, *ApJ*, 250, 478
- La Franca, F., et al. 2005, *ApJ*, 635, 864
- Laird, E. S., Nandra, K., Hobbs, A., & Steidel, C. C. 2006, *MNRAS*, 373, 217
- Lamer, G., Uttley, P., & McHardy, I. M. 2003, *MNRAS*, 342, L41
- Lutz, D., Maiolino, R., Spoon, H. W. W., & Moorwood, A. F. M. 2004, *A&A*, 418, 465
- Lutz, D., Valiante, E., Sturm, E., Genzel, R., Tacconi, L. J., Lehnert, M. D., Sternberg, A., & Baker, A. J. 2005, *ApJ*, 625, L83
- Magnelli, B., Chary, R. R., Pope, A., Elbaz, D., Morrison, G., & Dickinson, M. 2008, *ApJ*, 681, 258
- Maiolino, R., Salvati, M., Bassani, L., Dadina, M., della Ceca, R., Matt, G., Risaliti, G., & Zamorani, G. 1998, *A&A*, 338, 781
- Maiolino, R., Shemmer, O., Imanishi, M., Netzer, H., Oliva, E., Lutz, D., & Sturm, E. 2007, *A&A*, 468, 979
- Marconi, A., Risaliti, G., Gilli, R., Hunt, L. K., Maiolino, R., & Salvati, M. 2004, *MNRAS*, 351, 169
- Martínez-Sansigre, A., et al. 2007, *MNRAS*, 379, L6

- Matt, G., Brandt, W. N., & Fabian, A. C. 1996, *MNRAS*, 280, 823
- Matt, G., Fabian, A. C., Guainazzi, M., Iwasawa, K., Bassani, L., & Malaguti, G. 2000, *MNRAS*, 318, 173
- Matt, G., et al. 1997, *A&A*, 325, L13
- Menéndez-Delmestre, K., et al. 2007, *ApJ*, 655, L65
- Mulchaey, J. S., Koratkar, A., Ward, M. J., Wilson, A. S., Whittle, M., Antonucci, R. R. J., Kinney, A. L., & Hurt, T. 1994, *ApJ*, 436, 586
- Netzer, H., Mainieri, V., Rosati, P., & Trakhtenbrot, B. 2006, *A&A*, 453, 525
- Papovich, C., et al. 2007, *ApJ*, 668, 45
- Persic, M., Rephaeli, Y., Braito, V., Cappi, M., Della Ceca, R., Franceschini, A., & Gruber, D. E. 2004, *A&A*, 419, 849
- Polletta, M., Weedman, D., Hoenig, S., Lonsdale, C. J., Smith, H. E., & Houck, J. 2008, *ApJ*, 675, 960
- Polletta, M. d. C., et al. 2006, *ApJ*, 642, 673
- Pope, A., et al. 2008, *ApJ*, 675, 1171
- Ranalli, P., Comastri, A., & Setti, G. 2003, *A&A*, 399, 39
- Reddy, N. A., Steidel, C. C., Erb, D. K., Shapley, A. E., & Pettini, M. 2006, *ApJ*, 653, 1004
- Rees, M. J. 1984, *ARA&A*, 22, 471
- Rigopoulou, D., Spoon, H. W. W., Genzel, R., Lutz, D., Moorwood, A. F. M., & Tran, Q. D. 1999, *AJ*, 118, 2625
- Risaliti, G., Elvis, M., Fabbiano, G., Baldi, A., Zezas, A., & Salvati, M. 2007, *ApJ*, 659, L111
- Risaliti, G., Elvis, M., & Nicastro, F. 2002, *ApJ*, 571, 234
- Risaliti, G., Maiolino, R., & Salvati, M. 1999, *ApJ*, 522, 157
- Rosati, P., et al. 2002, *ApJ*, 566, 667
- Schmidt, M., & Green, R. F. 1983, *ApJ*, 269, 352
- Serjeant, S., Rawlings, S., Lacy, M., McMahon, R. G., Lawrence, A., Rowan-Robinson, M., & Mountain, M. 1998, *MNRAS*, 298, 321
- Shankar, F., Weinberg, D. H., & Miralda-Escudé, J. 2008, *ApJ*, in press (arXiv: 0710.4488v2)
- Shi, Y., et al. 2006, *ApJ*, 653, 127
- Spoon, H. W. W., Marshall, J. A., Houck, J. R., Elitzur, M., Hao, L., Armus, L., Brandl, B. R., & Charmandaris, V. 2007, *ApJ*, 654, L49
- Steffen, A. T., Brandt, W. N., Alexander, D. M., Gallagher, S. C., & Lehmer, B. D. 2007, *ApJ*, 667, L25
- Steffen, A. T., Strateva, I., Brandt, W. N., Alexander, D. M., Koekemoer, A. M., Lehmer, B. D., Schneider, D. P., & Vignali, C. 2006, *AJ*, 131, 2826
- Steidel, C. C., Adelberger, K. L., Shapley, A. E., Pettini, M., Dickinson, M., & Giavalisco, M. 2003, *ApJ*, 592, 728
- Steidel, C. C., Hunt, M. P., Shapley, A. E., Adelberger, K. L., Pettini, M., Dickinson, M., & Giavalisco, M. 2002, *ApJ*, 576, 653
- Steidel, C. C., Shapley, A. E., Pettini, M., Adelberger, K. L., Erb, D. K., Reddy, N. A., & Hunt, M. P. 2004, *ApJ*, 604, 534
- Sturm, E., Hasinger, G., Lehmann, I., Mainieri, V., Genzel, R., Lehnert, M. D., Lutz, D., & Tacconi, L. J. 2006, *ApJ*, 642, 81
- Suganuma, M., et al. 2006, *ApJ*, 639, 46
- Swinbank, A. M., Smail, I., Chapman, S. C., Blain, A. W., Ivison, R. J., & Keel, W. C. 2004, *ApJ*, 617, 64
- Szokoly, G. P., et al. 2004, *ApJS*, 155, 271
- Teplitz, H. I., et al. 2006, *ApJ*, 638, L1
- Tozzi, P., et al. 2006, *A&A*, 451, 457
- Treister, E., & Urry, C. M. 2005, *ApJ*, 630, 115
- Treister, E., et al. 2006, *ApJ*, 640, 603
- Valiante, E., Lutz, D., Sturm, E., Genzel, R., Tacconi, L. J., Lehnert, M. D., & Baker, A. J. 2007, *ApJ*, 660, 1060
- Vanden Berk, D. E., et al. 2001, *AJ*, 122, 549
- Vignali, C., Brandt, W. N., & Schneider, D. P. 2003, *AJ*, 125, 433
- Weedman, D., et al. 2006, *ApJ*, 653, 101
- Worsley, M. A., et al. 2005, *MNRAS*, 357, 1281
- Yaqoob, T. 1997, *ApJ*, 479, 184